Nanoscale

Cite this: *Nanoscale*, 2012, **4**, 5602

www.rsc.org/nanoscale

PAPER

Low-temperature synthesis of ZnO/CdS hierarchical nanostructure for photovoltaic application

Xue-Yan Chen, Tao Ling* and Xi-Wen Du*

Received 27th April 2012, Accepted 4th June 2012
DOI: 10.1039/c2nr31018j

Hierarchical nanostructures involving primary wide-band-gap nanowires and secondary narrow-band-gap branches are promising for photovoltaic application due to their excellent properties for light harvesting and fast carrier transport. In the present work, we developed a low-temperature process for facile synthesis of ZnO/CdS hierarchical nanowires, where the primary ZnO nanowires were first prepared *via* a hydrothermal route and then the secondary single-crystal CdS tips were grown on the ZnO nanowires by electrochemical deposition. The as-grown hierarchical ZnO/CdS nanowires are superior in charge separation as well as carrier transport, thus achieving higher open circuit voltage, short circuit current and final conversion efficiency than the common coaxial nanocables with CdS nanocrystal shell on core ZnO nanowires.

Introduction

Inspired by high-efficiency and low-cost dye-sensitized solar cells,[1,2] semiconductor nanocrystals have attracted much attention recently as an alternative to dyes for the construction of so-called semiconductor sensitized solar cells (SSSCs),[3] owing to their adjustable band gap, high stability, and multiple exciton generation effect.[4–6] On the other hand, single crystalline nanowire arrays were usually employed as the photoelectrode in SSSCs to load the semiconductor nanocrystals, because the one-dimensional (1D) nanostructure provides an ideal channel for effective carrier transport.[7] Particularly, ZnO nanowires are considered as the most favorable 1D material for solar conversion due to their high electron mobility and ease of crystallization.[8–10]

Up to now, several types of semiconductor nanocrystals, such as CdS,[11–13] CdSe,[14,15] CdTe,[16] Bi_2S_3, and PbS,[17] have been assembled onto the surface of ZnO nanowires to form a type II semiconductor heterojunction. Among them, CdS has drawn much attention because of its ideal band gap, relative stability and easy fabrication. Many techniques, for example, chemical bath deposition,[18] successive ionic layer adsorption and reaction,[19–21] molecular linking,[22,23] and electrochemical deposition,[16,24] have been developed to deposit multi-layered CdS nanoparticles onto the surface of ZnO nanowires and form coaxial ZnO/CdS nanowires (C-ZnO/CdS) shown in Fig. 1a.

Although ZnO nanowire-based SSSCs achieve a conversion efficiency of more than 4% by using CdS/CdSe co-sensitizers,[25,26] they suffer severe carrier loss due to the electron–hole recombination occurring at the interfaces between nanocrystals.[27] Hence, further improvement of the conversion efficiency requires a balance between enhancing the thickness of nanocrystal layer and minimizing the number of detrimental interfaces and defects.

One possible solution is to grow secondary single-crystal nanowires on primary semiconductor nanowires so as to form a so-called hierarchical structure.[28–33] Such a structure can drastically reduce the amount of interface as well as possess excellent carrier transport of 1D structure, thus efficiently depressing the recombination in multilayer nanoparticles. Hitherto, many hierarchical nanostructures, such as SnO_2/ZnO,[28] Si/InGaN,[29] TiO_2/CdS,[30] Si/ZnO,[31] and Si/TiO_2,[32] have been fabricated and applied in catalytic and photovoltaic fields. However, most of

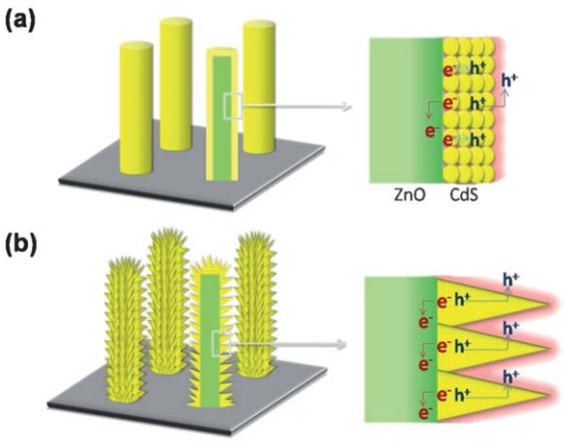

Fig. 1 Schematic diagram of the photoanodes consisting of H-ZnO/CdS and C-ZnO/CdS nanowire arrays on conductive glass substrate.

Tianjin Key Laboratory of Composite and Functional Materials, School of Materials Science and Engineering, Tianjin University, Tianjin 300072, P. R. China. E-mail: lingt04@tju.edu.cn; xwdu@tju.edu.cn

hierarchical nanostructures were grown from vapor phase at high temperatures,[29–32] which may destroy the conductive glass substrate of SSSCs. Hence, the well-developed high temperature techniques are hard to be incorporated into the fabrication of SSSCs.

In the present work, we proposed a low-temperature route to grow ZnO/CdS hierarchical nanostructures on a conductive glass substrate, where ZnO nanowire arrays were first synthesized on fluorine-doped tin oxide (FTO) glass by a hydrothermal route, and then single-crystal CdS nanotips were successfully grown on the primary ZnO nanowires by adopting an electrochemical deposition technique and carefully controlling the parameters. The schematic structure of the hierarchical ZnO/CdS nanowires (H-ZnO/CdS) is shown in Fig. 1b. These single crystalline nanotips without grain boundaries are superior in charge separation and carrier transport, and thus achieve a higher overall conversion efficiency than C-ZnO/CdS nanowires.

Experimental

Synthesis of H-ZnO/CdS and C-ZnO/CdS structures

ZnO nanowires on conductive glass substrate were fabricated using a hydrothermal route.[34,35] Firstly, a ZnO seed layer was deposited on a FTO substrate by a dip-coating method. Afterwards, ZnO nanowires arrays were grown in an aqueous solution of 0.025 M zinc nitrate hexahydrate ($Zn(NO_3)_2 \cdot 6H_2O$) and 0.025 M hexamethylenetetramine (HMT) heated at 90 °C for 9 h.

CdS nanocrystals were grown on the ZnO nanowires by electrochemical deposition. In a typical procedure, a dimethyl sulfoxide (DMSO) solution containing 0.055 M cadmium chloride ($CdCl_2$) and 0.19 M sulfur (S) was used as precursor.[36] The CdS nanocrystal multilayer and single-crystal CdS nanotips were deposited galvanostatically at a current density of 5 mA cm^{-2} for 15 s to 1 min, and 0.5–1 mA cm^{-2} for 3 to 8 min, respectively, at 110 °C in a two-electrode electrochemical cell, with the nanowire arrays on FTO glass as the cathode and platinum metal as the counter electrode.

Cell assembly

The photoanodes with an effective area of 0.24 cm^2 were assembled and sealed with a transparent hot-melt surlyn ring to the counter electrodes (Pt-coated FTO glass). The iodide-based electrolyte, consisting of 0.5 M LiI, 0.05 M I_2, 0.3 M *tert*-butylpyridine, and 0.3 M tetrabutylammonium iodide in acetonitrile, was injected into the interelectrode space from the counter electrode side through a predrilled hole.

Characterization

The photoanode morphology was observed using a Hitachi S-4800 scanning electron microscope (SEM) equipped with energy-dispersive X-ray spectroscopy (EDS) module and a FEI TechnainG2 F20 transmission electron microscope (TEM) with a field-emission gun operating at 200 kV. The X-ray diffractometry (XRD) for the crystal structure of the products was carried out in a Bruker D8 advance. UV-vis absorption spectra were recorded on a Hitachi 3010 spectrophotometer. Photocurrent density–voltage (J–V) curves were recorded using a Keithley 2611 digital multimeter. The light source was a 150 W xenon lamp (Sciencetech, SS150) calibrated to 100 mW cm^{-2} with a standard Si solar cell. Electrochemical impedance spectra (EIS) measurements were carried out at a constant temperature of 20 °C under dark condition, using a Princeton Versa Stat3 electrochemistry workstation. The EIS spectra were obtained at a forward bias of 0–0.3 V at frequencies ranging from 0.05 Hz to 200 kHz and the oscillation potential amplitudes of 10 mV.

Results and discussion

Fig. 2a shows a typical SEM image of the as-grown ZnO nanowire arrays on a FTO substrate. The ZnO nanowires exhibit a regular hexagonal shape with diameters of 60–100 nm and lengths of 2 μm (Fig. 2a, inset). After electrochemical deposition of CdS at a current density of 0.8 mA cm^{-2} for 4 min, the surface of ZnO nanowires becomes rough and their diameters increase approximately to 200–250 nm (Fig. 2b). The high magnification SEM and TEM images (Fig. 2c and d) clearly illustrate the mace-like H-ZnO/CdS hierarchical nanostructures with nanotips coated on ZnO nanowires. The high resolution TEM (HRTEM) image illustrates that the CdS nanotip is single crystalline with a length about 50 nm (Fig. 2e). The enlarged image of the tip is shown in Fig. 2f. Lattice fringes corresponding to {102} planes of wurtzite CdS are clearly observed, indicating that the CdS nanotips are highly crystalline. In order to observe the interface between ZnO and CdS clearly, the electrodeposition was interrupted at 1 min so as to obtain CdS buds at the early growth stage. Fig. 2f shows that the CdS bud grows directly on the ZnO nanorod with continuous atomic layer across the interface, which can effectively decrease the interface resistance between ZnO and CdS.

For comparison, a compact and uniform layer of CdS nanocrystals was formed on ZnO nanowires when electrochemical deposition was conducted at a large current density (5 mA cm^{-2}). The diameter of C-ZnO/CdS nanowires is smaller than that of H-ZnO/CdS, as shown in the SEM image of Fig. 3a. The TEM image in Fig. 3b indicates that the coating layer is composed of stacking CdS nanoparticles. Fig. 4a presents EDS spectra of pure ZnO, H-ZnO/CdS, and C-ZnO/CdS nanowires, which demonstrate that the coating layer in C-ZnO/CdS and H-ZnO/CdS structures is composed of Cd and S elements. The crystal structures of the three types of nanowires were verified by XRD characterization, the spectra being shown in Fig. 4b. For pure ZnO nanowire arrays, the diffraction peaks can be indexed to (100), (002), (101), (102) and (110) planes, respectively, of wurtzite ZnO (JCPDS file no. 36-1451). After electrodeposition of CdS nanotips and CdS nanoparticles, four new diffraction peaks centered at 24.8, 26.5, 28.2 and 43.7° are observed, which can be indexed respectively to (100), (002), (101) and (110) planes of CdS wurtzite structure (JCPDS no. 41-1049).

Although different CdS nanostructures, such as nanoconifers and nanowires, have been synthesized on ITO substrate by electrochemical deposition,[37,38] to the best of our knowledge, the hierarchical structure of CdS nanotips on ZnO nanowires has never been reported. To investigate the formation mechanism of CdS nanotips, the electrochemical deposition was conducted at different current densities. It was found that single-crystal nanotips could only be obtained at low current densities, from

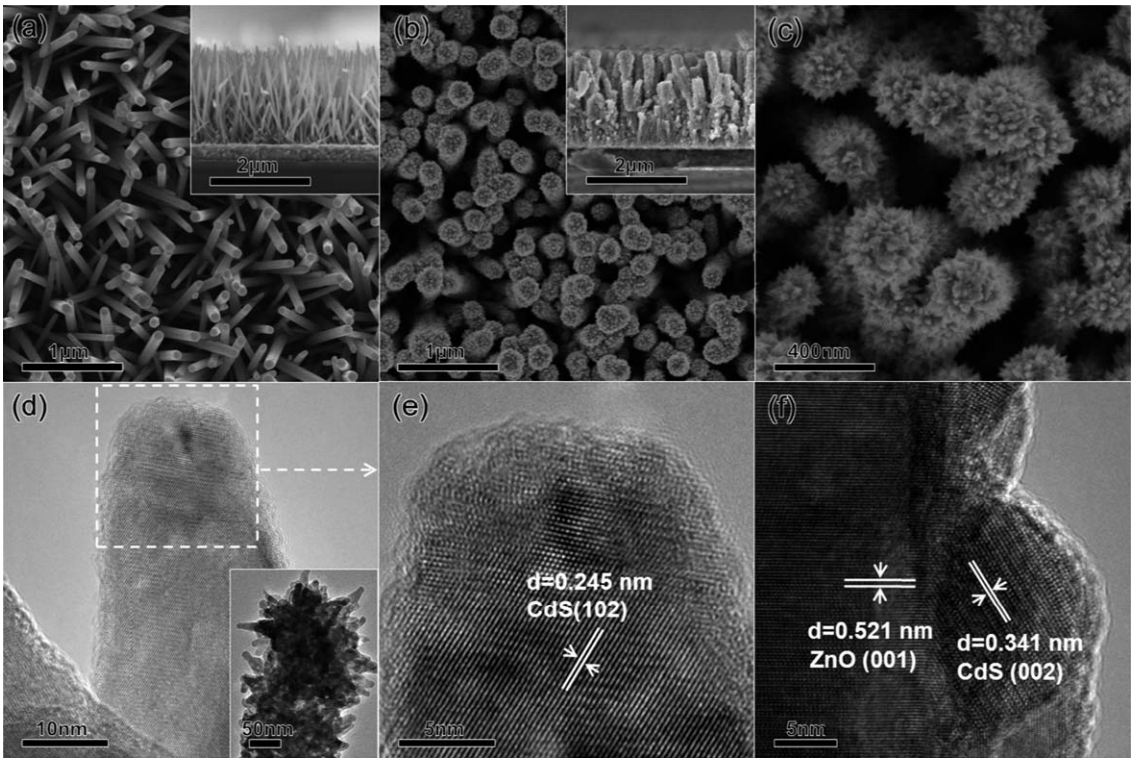

Fig. 2 SEM and TEM images of as-synthesized H-ZnO/CdS. (a) Top view of ZnO nanowires; the inset is a cross-sectional SEM image. (b) Top view of H-ZnO/CdS; the inset is a cross-sectional SEM image. (c) The high-magnification SEM of H-ZnO/CdS. (d) HRTEM image of the H-ZnO/CdS structure; the inset is a low magnification TEM image. (e) The enlarged image of the rectangular region in (d). (f) HRTEM image of the interface between ZnO nanowire and CdS bud at the early growth stage.

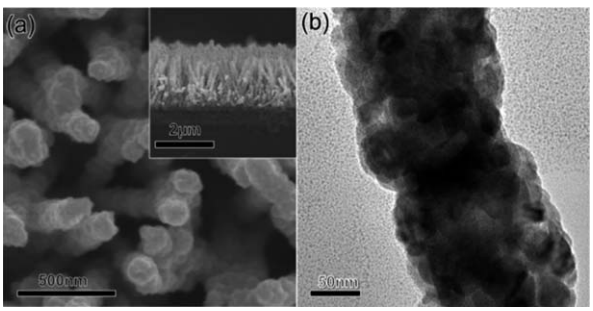

Fig. 3 SEM and TEM images of as-synthesized C-ZnO/CdS. (a) Top view of C-ZnO/CdS, the inset is a cross-sectional SEM image. (b) TEM image of C-ZnO/CdS.

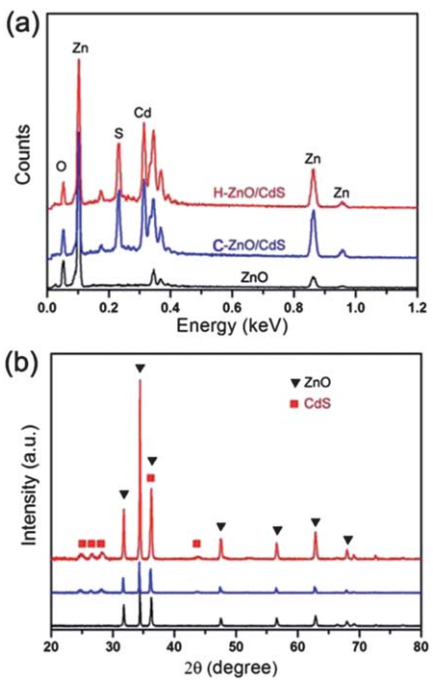

Fig. 4 (a) EDS results of pure ZnO, H-ZnO/CdS and C-ZnO/CdS nanowires. (b) XRD patterns of pure ZnO, H-ZnO/CdS and C-ZnO/CdS nanowires.

0.5 to 1 mA cm^{-2}, and grew gradually from a smooth CdS layer on ZnO nanowires (Fig. 5a–c). In contrast, when the current density was over 1 mA cm^{-2}, *e.g.* at 5 mA cm^{-2}, CdS particles deposited rapidly on the ZnO nanowires, resulting in a rough surface in 15 seconds; further deposition plastered the surface and led to a compact CdS layer consisting of nanoparticles in 45 seconds (Fig. 5d–f).

It has been proven that the current density determines the ion immigration velocity and nucleation rate in the electrochemical deposition process.[34–36] In case of CdS electrodeposition, the reduction of S atoms and then the formation of S^{2-} ions are subject to the current density. Specifically, at low current density, the slow and steady generation and diffusion of S^{2-} ions

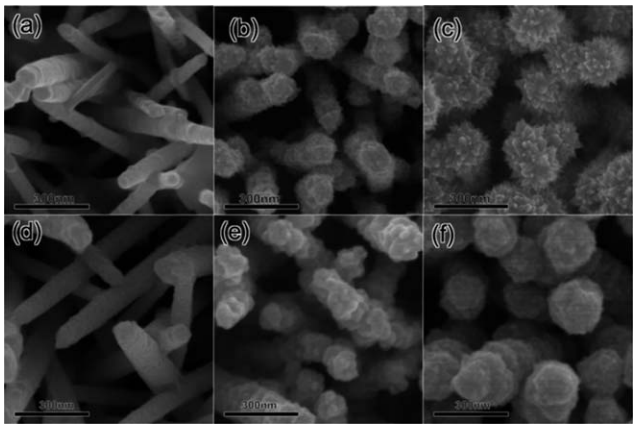

Fig. 5 SEM images of ZnO/CdS structures prepared with different current density and time: (a) 0.8 mA cm^{-2} for 1 min, (b) 0.8 mA cm^{-2} for 1.5 min, (c) 0.8 mA cm^{-2} for 4.5 min, (d) 5 mA cm^{-2} for 8 s, (e) 5 mA cm^{-2} for 15 s and (f) 5 mA cm^{-2} for 45 s.

dominate the CdS growth in some polar planes which have low nucleation energy.[36,37] As a result, single-crystal CdS nanotips grow from the surface of ZnO nanowires. In comparison, a high current density generates a high concentration of S^{2-} ions and high ion velocity,[38] which causes a rapid growth of CdS nanocrystals in an isotropic way. Hence, as-electrodeposited CdS exhibits a particle shape and forms a compact layer. Thus, the ion immigration velocity and nucleation rate are the key factors to gain single-crystal nanotips by electrodeposition. It is believed that this facile methodology can be expanded to fabricate other hierarchical nanostructures, such as CdSe or CdTe, on oxide nanorods.

In order to evaluate the photovoltaic performance of the H-ZnO/CdS structure, we took the C-ZnO/CdS structure as a reference. First of all, the light absorption capabilities of the two structures were equated by precisely adjusting the electrodeposition parameters. Specifically, the H-ZnO/CdS structure was fabricated with a current density of 0.8 mA cm^{-2} for 4 min, while its C-ZnO/CdS counterpart was made with a current density of 5 mA cm^{-2} for 35 s. The overlapping absorption spectra (Fig. 6) and the quantitative EDS analysis (Table 1) for the two structures demonstrate that their absorption capabilities are almost the same.

Table 1 The quantitative EDS results of H-ZnO/CdS and C-ZnO/CdS structures

Sample	Cd (at%)	S (at%)	Zn (at%)
H-ZnO/CdS	23.44	24.08	52.48
C-ZnO/CdS	23.41	24.08	52.51

Next, the two structures were assembled into solar cells and compared in terms of their photo-electron conversion efficiency. The measured photocurrent density–voltage (J–V) characteristics are shown in Fig. 7, and the related physical values, including V_{OC} (open circuit voltage), J_{SC} (short circuit current), FF (fill factor), and η (light to electricity conversion efficiency), are summarized in Table 2. The η value can be evaluated from the equation $\eta = (J_{SC} \times V_{OC} \times FF)/P_{in}$, where P_{in} is the incident light power density. As shown in Fig. 7 and Table 2, the H-ZnO/CdS sample exhibits larger values of J_{SC}, V_{OC}, and overall conversion efficiency. Since the absorption ability of the two structures is almost the same, the photovoltaic results indicate that the H-ZnO/CdS structure is advantageous over the C-ZnO/CdS structure in charge separation and collection.

To clarify the origin of the different performance, electrochemical impedance spectra (EIS) measurements were performed at different negative biased voltages in dark condition,[39–41] and the results are shown in Fig. 8a and b. The spectra enlarged in the high frequency range (Fig. 8b) presented the Warburg behaviour characteristic of a transmission line. Thus, the transmission line equivalent circuit shown in Fig. 8c was employed to fit the EIS results.[42,43] The model involves some important parameters of photoanode, such as the electron resistance, R_t ($R_t = r_t/l$), the interfacial resistance R_{ct} ($R_c = r_{ct}/l$), the chemical capacitance, C_μ ($C_\mu = c_\mu l$), where r_t, r_{ct}, and c_μ are parameters of the transmission line model, and l is the thickness of the photoanode. The resistance of the electrolyte is modelled by a finite Warburg element W_s, and R_{Pt}, C_{Pt} are the interface charge transfer resistance and chemical capacitance between the Pt counter electrode and electrolyte, respectively. Similarly, the resistance and chemical capacitance between the exposed FTO and electrolyte are described by R_{FTO} and C_{FTO}, respectively.

The potential dependence of the transmission line parameters was extracted from the EIS fits and shown in Fig. 9. Fig. 9a represents the typical behavior of the capacitance in the two structures, which is related to electronic carrier accumulation

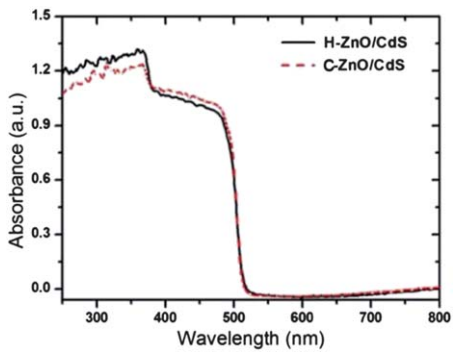

Fig. 6 Absorption spectra of H-ZnO/CdS and C-ZnO/CdS structures.

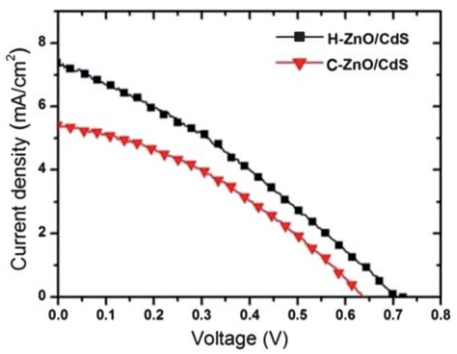

Fig. 7 J–V curves of H-ZnO/CdS and C-ZnO/CdS structures.

Table 2 *J–V* characteristics of H-ZnO/CdS and C-ZnO/CdS structures

Sample	V_{OC} (mV)	J_{SC} (mA cm^{-2})	FF	η (%)
H-ZnO/CdS	0.70	7.38	0.31	1.62
C-ZnO/CdS	0.63	5.35	0.37	1.25

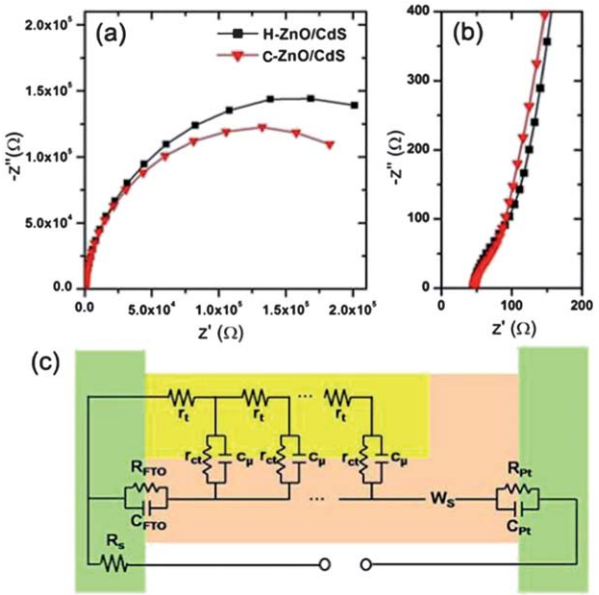

Fig. 8 (a) Impedance measurements of H-ZnO/CdS and C-ZnO/CdS at bias voltage of −0.21 V under dark conditions. (b) Zoom of graph (a). (c) The equivalent circuit employed to model the tested SSSC structures.

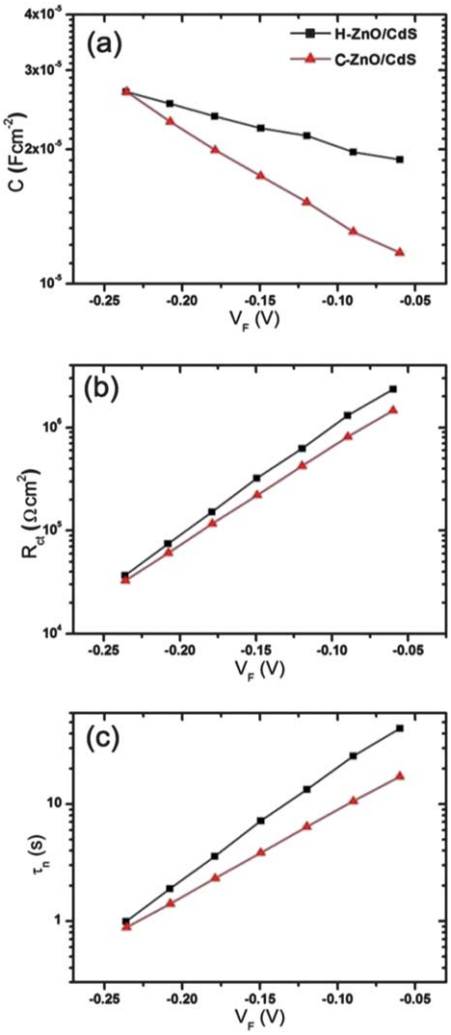

Fig. 9 Impedance characterizations of H-ZnO/CdS and C-ZnO/CdS structures: (a) the chemical capacitance, C_μ, (b) recombination resistance, R_{ct}, and (c) electron lifetime, τ_n.

and distribution in the photoanode based on the equation $C_\mu = ne^2/kT$, where k is the Boltzmann constant, T the temperature, and e the electron charge.[38] Obviously, the H-ZnO/CdS structure exhibits a larger value of C_μ than that of the C-ZnO/CdS structure, indicating that the H-ZnO/CdS structure can efficiently accumulate charges and thus enhance the density of free electrons. This result is consistent with the larger value of J_{SC} observed in the H-ZnO/CdS structure.

Moreover, the higher interface resistance (R_{ct}) of the H-ZnO/CdS structure in Fig. 9b suggests its advantage over the C-ZnO/CdS structure in retarding charge recombination, which is understandable because single-crystal nanotips can facilitate electron transport and injection from the CdS layer to the ZnO nanowire core. In contrast, photo-generated electrons in the C-ZnO/CdS anode are easily trapped and recombined at the interfaces of CdS nanoparticles (Fig. 3b), causing a severe carrier loss and the reduction of photo-voltage (Fig. 7 and Table 2). Additionally, the electron lifetime, τ_n, can be determined by $\tau_n = R_c \times C_\mu$. As shown in Fig. 9c, the τ_n for the H-ZnO/CdS structure is longer than that for its C-ZnO/CdS counterpart, which contributes directly to the higher J_{SC} and overall conversion efficiency.

Based on the EIS results, we can conclude that compared with CdS nanoparticles, single crystalline CdS nanotips are superior in charge separation and accumulation, as well as carrier transport. Thus the H-ZnO/CdS structure achieves a higher open circuit voltage, short circuit current and final conversion efficiency.

Conclusions

CdS single crystalline nanotips were electrochemically grown on the surface of ZnO nanowires at ambient temperature. The hierarchical ZnO/CdS nanowires show superior charge separation and collection, as well as carrier transport by depressing possible recombination, thus achieving higher open circuit voltage, short circuit current and final conversion efficiency in comparison with the common coaxial nanocables with CdS nanocrystal shell and ZnO core. Our experimental results indicate that the unique CdS nanotips can serve as a potential substitute for common nanoparticulate sensitizers in SSSCs. Further efficiency promotion can be anticipated by prolonging the length of ZnO nanowires to load more CdS nanotips, coating a hole transfer layer onto the surface of CdS nanotips to facilitate charge separation, and replacing the nanotip materials with

those with a narrower band gap, such as CdSe or CdTe, to enhance light absorption.

Acknowledgements

This work was supported by the Natural Science Foundation of China (no. 51102176, 50972102 and 50902103), National High-tech R&D Program of China (no 2009AA03Z301), Research Fund for the Doctoral Program of Higher Education of China (no 20100032120021), and Natural Science Foundation of Tianjin City (no. 11JCYBJC02000, 09JCZDJC22600 and 08JCYBJC02900).

Notes and references

1 M. Gratzel, *Nature*, 2001, **414**, 338–344.
2 J. Mao, J.-J. Li, T. Ling, H. Liu, J. Yang and X.-W. Du, *Nanotechnology*, 2011, **22**, 245604.
3 P. V. Kamat, *J. Phys. Chem. C*, 2008, **112**, 18737–18753.
4 S. Ruhle, M. Shalom and A. Zaban, *ChemPhysChem*, 2010, **11**, 2290–2304.
5 R. D. Schaller and V. I. Klimov, *Phys. Rev. Lett.*, 2004, **92**, 186601.
6 Z. Yang, C.-Y. Chen, P. Roy and H.-T. Chang, *Chem. Commun.*, 2011, **47**, 9561–9571.
7 K. Yu and J. Chen, *Nanoscale Res. Lett.*, 2009, **4**, 1–10.
8 L. E. Greene, M. Law, D. H. Tan, M. Montano, J. Goldberger, G. Somorjai and P. D. Yang, *Nano Lett.*, 2005, **5**, 1231–1236.
9 K. Keis, C. Bauer, G. Boschloo, A. Hagfeldt, K. Westermark, H. Rensmo and H. Siegbahn, *J. Photochem. Photobiol., A*, 2002, **148**, 57–64.
10 J. Qiu, X. Li, F. Zhuge, X. Gan, X. Gao, W. He, S.-J. Park, H.-K. Kim and Y.-H. Hwang, *Nanotechnology*, 2010, **21**, 195602.
11 T. Ling, M.-K. Wu, K.-Y. Niu, J. Yang, Z.-M. Gao, J. Sun and X.-W. Du, *J. Mater. Chem.*, 2011, **21**, 2883–2889.
12 X. Song, X.-L. Yu, Y. Xie, J. Sun, T. Ling and X.-W. Du, *Semicond. Sci. Technol.*, 2010, **25**, 095014.
13 Y. Tak, H. Kim, D. Lee and K. Yong, *Chem. Commun.*, 2008, 4585–4587.
14 Z. Lu, J. Xu, X. Xie, H. Wang, C. Wang, S.-Y. Kwok, T. Wong, H. L. Kwong, I. Bello, C.-S. Lee, S.-T. Lee and W. Zhang, *J. Phys. Chem. C*, 2012, **116**, 2656–2661.
15 X. Qiu, W. Que, X. Yin, J. Zhang and J. Chen, *Semicond. Sci. Technol.*, 2011, **26**, 095028.
16 X. Wang, H. Zhu, Y. Xu, H. Wang, Y. Tao, S. Hark, X. Xiao and Q. Li, *ACS Nano*, 2010, **4**, 3302–3308.
17 R. Vogel, P. Hoyer and H. Weller, *J. Phys. Chem.*, 1994, **98**, 3183–3188.
18 W. Lee, S. K. Min, V. Dhas, S. B. Ogale and S.-H. Han, *Electrochem. Commun.*, 2009, **11**, 103–106.
19 J. Joo, D. Kim, D.-J. Yun, H. Jun, S.-W. Rhee, J. S. Lee, K. Yong, S. Kim and S. Jeon, *Nanotechnology*, 2010, **21**, 325604.
20 H. Lee, M. Wang, P. Chen, D. R. Gamelin, S. M. Zakeeruddin, M. Graetzel and M. K. Nazeeruddin, *Nano Lett.*, 2009, **9**, 4221–4227.
21 Y. Tak, S. J. Hong, J. S. Lee and K. Yong, *J. Mater. Chem.*, 2009, **19**, 5945–5951.
22 W.-T. Sun, Y. Yu, H.-Y. Pan, X.-F. Gao, Q. Chen and L.-M. Peng, *J. Am. Chem. Soc.*, 2008, **130**, 1124–1125.
23 I. Mora-Sero, S. Gimenez, F. Fabregat-Santiago, R. Gomez, Q. Shen, T. Toyoda and J. Bisquert, *Acc. Chem. Res.*, 2009, **42**, 1848–1857.
24 M. Zhou, H. Zhu, X. Wang, Y. Xu, Y. Tao, S. Hark, X. Xiao and Q. Li, *Chem. Mater.*, 2010, **22**, 64–69.
25 M. Seol, H. Kim, Y. Tak and K. Yong, *Chem. Commun.*, 2010, **46**, 5521–5523.
26 J. Xu, X. Yang, H. Wang, X. Chen, C. Luan, Z. Xu, Z. Lu, V. A. L. Roy, W. Zhang and C.-S. Lee, *Nano Lett.*, 2011, **11**, 4138–4143.
27 G. Hodes, *J. Phys. Chem. C*, 2008, **112**, 17778–17787.
28 C. Cheng, B. Liu, H. Yang, W. Zhou, L. Sun, R. Chen, S. F. Yu, J. Zhang, H. Gong, H. Sun and H. J. Fan, *ACS Nano*, 2009, **3**, 3069–3076.
29 Y. J. Hwang, C. H. Wu, C. Hahn, H. E. Jeong and P. Yang, *Nano Lett.*, 2012, **12**, 1678–1682.
30 J.-C. Lee, T. G. Kim, W. Lee, S.-H. Han and Y.-M. Sung, *Cryst. Growth Des.*, 2009, **9**, 4519–4523.
31 P. Sudhagar, T. Song, D. H. Lee, I. Mora-Sero, J. Bisquert, M. Laudenslager, W. M. Sigmund, W. I. Park, U. Paik and Y. S. Kang, *J. Phys. Chem. Lett.*, 2011, **2**, 1984–1990.
32 J. Shi, Y. Hara, C. Sun, M. A. Anderson and X. Wang, *Nano Lett.*, 2011, **11**, 3413–3419.
33 I. S. Cho, Z. Chen, A. J. Forman, D. R. Kim, P. M. Rao, T. F. Jaramillo and X. Zheng, *Nano Lett.*, 2011, **11**, 4978–4984.
34 Y. Lee, Y. Zhang, S. L. G. Ng, F. C. Kartawidjaja and J. Wang, *J. Am. Ceram. Soc.*, 2009, **92**, 1940–1945.
35 X.-L. Yu, J.-G. Song, Y.-S. Fu, Y. Xie, X. Song, J. Sun and X.-W. Du, *J. Phys. Chem. C*, 2010, **114**, 2380–2384.
36 D. S. Xu, Y. J. Xu, D. P. Chen, G. L. Guo, L. L. Gui and Y. Q. Tang, *Chem. Phys. Lett.*, 2000, **325**, 340–344.
37 Z. Feng, Q. Zhang, L. Lin, H. Quo, J. Zhou and Z. Lin, *Chem. Mater.*, 2010, **22**, 2705–2710.
38 Y.-X. Nan, F. Chen, L.-G. Yang and H.-Z. Chen, *J. Phys. Chem. C*, 2010, **114**, 11911–11917.
39 Q. Wang, S. Ito, M. Graetzel, F. Fabregat-Santiago, I. Mora-Sero, J. Bisquert, T. Bessho and H. Imai, *J. Phys. Chem. B*, 2006, **110**, 25210–25221.
40 F. Fabregat-Santiago, G. Garcia-Belmonte, I. Mora-Sero and J. Bisquert, *Phys. Chem. Chem. Phys.*, 2011, **13**, 9083–9118.
41 F. Fabregat-Santiago, J. Bisquert, G. Garcia-Belmonte, G. Boschloo and A. Hagfeldt, *Sol. Energy Mater. Sol. Cells*, 2005, **87**, 117–131.
42 M. K. Wu, T. Ling, Y. Xie, X. G. Huang and X. W. Du, *Semicond. Sci. Technol.*, 2011, **26**, 105001.
43 V. Gonzalez-Pedro, X. Xu, I. Mora-Sero and J. Bisquert, *ACS Nano*, 2010, **4**, 5783–5790.